A Birdcage Coil Tuned by RF Shielding for Application at 9.4 T

Bernard J. Dardzinski,* Shizhe Li,* Christopher M. Collins,*,† Gerald D. Williams,* and Michael B. Smith,*,‡

*Department of Radiology, Center for NMR Research, and ‡Department of Cellular and Molecular Physiology, Pennsylvania State University College of Medicine, Hershey, Milton S. Hershey Medical Center, Hershey, Pennsylvania 17033; and †Department of Bioengineering, University of Pennsylvania, Philadelphia, Pennsylvania 19104

The design and performance of an inductively fed low-pass birdcage radiofrequency (RF) coil for applications at 9.4 T are described where tuning is accomplished by mechanically moving a concentric RF shield about the longitudinal axis of an RF coil. Moving the shield about the RF coil effectively changes the mutual inductance of the system, providing a mechanism for adjusting the resonant frequency. RF shield tuning eliminates adjustable capacitors on the legs of the RF coil, eliminates current imbalances and field distortions, and results in improved B_1 field homogeneity and high quality (Q) factors. RF shield tuning and inductive matching provide an isolated resonance structure which is both physically and electrically unattached. Experimental analysis of shield position on both B_1 field homogeneity and resonant frequency is provided. Computer simulations of B_1 field homogeneity as a function of shield position and shield diameter are also presented. Magnetic resonance microimaging substantiates the usefulness of this design. © 1998 Academic Press

Key Words: birdcage coil; RF shield; mutual inductance; magnetic resonance imaging.

INTRODUCTION

Birdcage radiofrequency (RF) coils are preferred for use in MRI because of their excellent RF magnetic (B_1) field homogeneity (*1*). Building these types of coils for applications at higher static magnetic field strengths (9.4 T) is more difficult than for larger coils operating at lower frequencies (1–2 T). This difficulty arises because the capacitance (as well as the inductance) of the circuit must be made quite small to ensure that the coil will resonate at the required frequency. At these high frequencies, the impedance of all legs should be equivalent in order to provide the proper sinusoidal current distribution necessary to produce excellent B_1 field homogeneity.

Small low-pass birdcage RF coils (diameter = 1–3 cm) with adjustable capacitors for tuning and matching on the legs are difficult to construct. Adjustable capacitors require a significant amount of a space for their placement. Adjustable capacitors also add inductance, create a larger circuit path, and create field distortions arising from current imbalances in birdcage coils (*2*). High-pass birdcage coils could also

be built for application in a vertical-bore 9.4-T MRI system, thus alleviating the need to place adjustable capacitors on the legs of the coil. Their use, however, would still place physical limitations on construction and degrade coil performance.

RF shields are typically used to reduce the interaction between an RF coil and other hardware within the MRI system. RF shields reduce noise and therefore help to improve the signal-to-noise ratio (SNR) of the NMR experiment. RF shields also provide a stable environment to tune and match the RF coil. RF shield technology was employed to effectively change the inductance of a low-pass birdcage coil to circumvent the need for adjustable tuning capacitors. Shielding decreases the effective inductance of a circuit, causing the resonant frequency to increase (*3, 4*).

In this work, a low-pass birdcage coil with an RF shield on a cylindrical former which mechanically moves coaxial about the longitudinal axis of an RF coil was constructed. The resonant frequency changes as a function of the shield's position in relation to the RF coil. Tuning of the circuit can be controlled by changing the effective inductance. Simple mechanical tuning by use of an adjustable RF shield eliminates the physical constraints of adjustable tuning capacitors and more effectively maintains the sinusoidal distributed current pattern necessary for optimum B_1 field homogeneity. This design has led to a useful RF coil for applications in neonatal rat pup brain imaging and gradient-localized spectroscopy at 9.4 T.

THEORY

Although the exact analytical solution to explain the change in resonance frequency with shield coverage about an RF coil is beyond the scope of this paper, it can be most easily understood as a change in mutual inductance between the RF coil and shield. A detailed analysis of mutual inductance and shield geometry on resonant frequency has been addressed previously (*3, 5–9*) and the relationships between birdcage coil circuit parameters and the resonant frequency have been described in detail elsewhere (*6–11*).

For our purpose, a qualitative relationship between the coil's resonant frequency, ν, and the effective inductance, L_{eff}, can be simply expressed as

$$\nu \propto \frac{1}{\sqrt{L_{eff}}} .$$ [1]

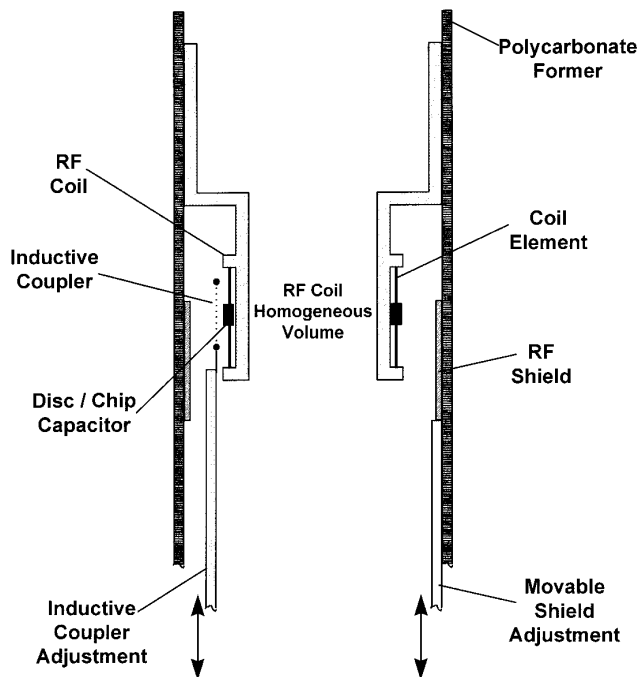For a shielded RF coil, L_{eff} can be written as

$$L_{eff} = L' - kM,$$ [2]

where L' is the coil inductance without any RF shielding present, and M is the mutual inductance between the conducting elements of the RF coil and the RF shield. The L' term includes the contribution of the self-inductance of conducting elements and the mutual inductance contribution between these elements and excludes the effects of the shield. Mathematically, the RF shield can be replaced by the mirror image of the conducting elements and M then becomes the mutual inductance between the coil elements and the mirror elements. The factor k denotes the ratio of the current in the mirror elements to the current in the conducting elements. The currents in the mirrored coil elements flow in the opposite direction to the current in the coil's elements which is indicated by the negative sign in Eq. [2].

When the shield is moved along the longitudinal axis away from the geometrical center of the RF coil the mutual inductance between the coil elements and shield decreases. This increases the effective inductance and lowers the resonant frequency. When the RF shield is symmetrically centered about the RF coil, the mutual inductance is maximum, which results in the minimum effective inductance and the highest resonant frequency.

Recently, Collins et al. have modeled and experimentally verified the effects of shield geometry on both the B_1 field strength and the homogeneity in the birdcage coil (8). Not only is the length of the shield important in assessing coil performance but the relationship between the shield and coil diameters is also significant. Their results indicate that the B_1 field strength diminishes as shield diameter decreases and shield length increases. This knowledge of field behavior as a function of shield geometry has led to the design and fabrication of an RF birdcage coil for application at 9.4 T where tuning is accomplished by an adjustable RF shield.

MATERIALS AND METHODS

A 26×24-mm (length $\times$ diameter) Delrin former was machined to construct a low-pass birdcage coil. Eight nonmagnetic capacitors (3.3 pF; TTI, Moorestown, NJ) were placed at equidistant positions around the cylindrical former. Coil elements were composed of only the disc capacitors. End-ring segments were constructed from the leads of the
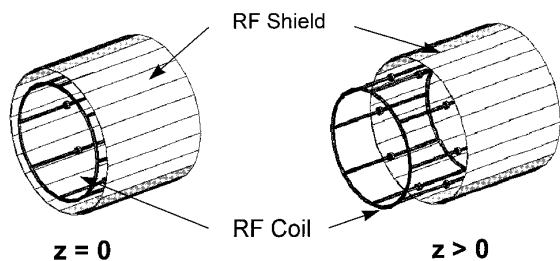

FIG. 1. Schematic cross-sectional representation of the RF coil with an RF shield and an inductive coupler. The RF shield was used to tune the coil to the appropriate resonant frequency by changing the effective inductance. The position of the inductive coupler determines the 50-ohm match of the circuit. The polycarbonate former containing RF coil and sample can be removed from the bottom of the magnet without removing the microimaging gradient insert.

same capacitors. The shield (25.4 mm in length) was constructed from copper foil tape fixed around a polycarbonate former. Matching was accomplished through inductive coupling as illustrated in Fig. 1. This diagram represents the cross section of the RF probe with an adjustable shield used for tuning (resonant frequency) adjustment. The RF shield of the microimaging gradient insert is not shown in the diagram.

Measurements of frequency versus shield position were performed using an HP 4195A Network/Spectrum analyzer. The reference point, $z = 0$ mm, for these measurements was where the shield was symmetric about the longitudinal axis of the RF coil (Fig. 2) with respect to the longitudinal center of the RF coil. The z position is defined to increase from zero when the center of the longitudinal axis of the RF shield moves toward the end ring of the RF coil. Shifts in frequency versus position were measured for two different shield diameters (D_s), 31 and 36 mm or 1.3 and 1.5 times the diameter of the RF coil (D_c), respectively. Measurements were performed both with and without the 45-mm-diameter shield (length = 170 mm) of the microimaging gradient insert. Images were acquired on a Bruker AM400 wide-bore spectrometer operating at 400 MHz for ^{1}H.

By combining birdcage theory and a method of three-

FIG. 2. Three-dimensional representation of both the RF shield and the RF coil as a function of position along the longitudinal (z) axis of the RF coil. As z is made greater than zero the mutual inductance between the coil and shield decreases, increasing the effective inductance which will lower the resonant frequency. This model was used for computer simulations. The $z = 0$ position is defined as the position where the RF shield is symmetric about the longitudinal axis of RF coil and is referenced to the geometrical center of the RF coil.

dimensional (3D) finite element analysis, B_1 field strength was calculated in all space as a function of shield position and shield to coil diameter ratio (D_s/D_c). All calculations of field patterns were made using Maxwell 3D field simulator software (Ansoft Corp., Pittsburgh, PA) on an IBM RISC 6000, Model 550, computer with 256 MB of DRAM (*8*).

Shaded contour plots were then made on a sagittal ($x–z$) plane through which end-ring currents were at a minimum. Five different contours were chosen to represent the relative deviation of the B_1 field magnitude in reference to the center of the coil: 0–10, 10–30, 30–50, 50–70, and >70%. The area and centroid of these contours were calculated to compare B_1 field homogeneity as a function of shield diameter and shield position.
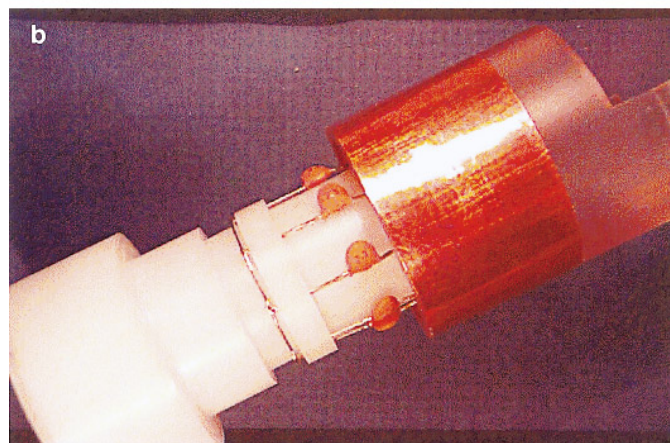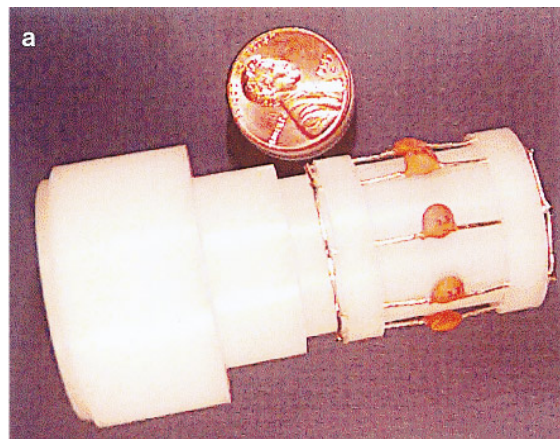
RESULTS AND DISCUSSION

Photographs of the RF coil and RF coil with an adjustable RF shield are shown in Figs. 3a and 3b, respectively. The coil was simply and inexpensively constructed from eight disc capacitors as depicted in Fig. 3a. Capacitance or coil length can be adjusted to ensure the proper resonant frequency. The shielding effect of the microimaging gradients must be accounted for when choosing proper coil length and capacitance. The inductive feed and RF shield are moved simply by mechanical rods. The RF coil and shield are positioned within a polycarbonate tube which is then inserted into the vertical-bore magnet from the bottom. This allows the sample to be easily and reproducibly changed without removal of the microimaging gradient insert.

Jin *et al.* have indicated that the current imbalance in the legs of a birdcage coil can lead to loss of field homogeneity (*2*). This is especially true for the coil presented here in the low-pass configuration. Each capacitance was only 3.3 pF and a small deviation can lead to imperfect operation. The coil can also be constructed using ceramic
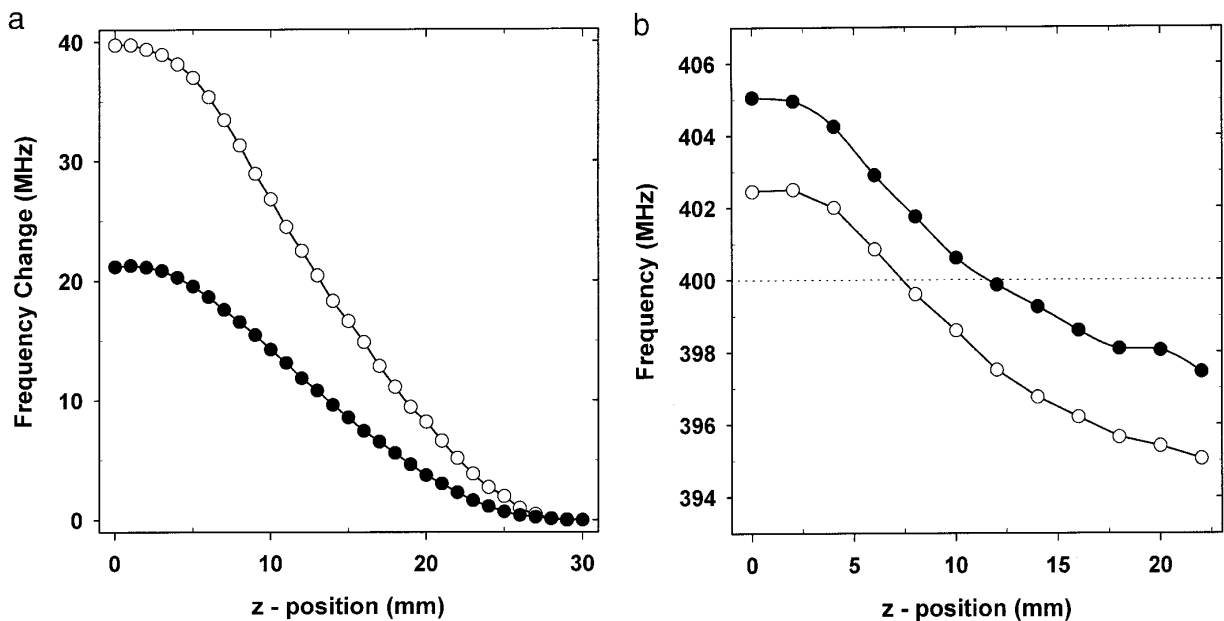
chip capacitors, which normally have better tolerances, providing the preferred current distribution and increased B_1 field homogeneity.

Measured resonant frequency change versus shield position is depicted in Fig. 4a. Data in Fig. 4a were made for two different shield diameters. The relative position of the coil to the shield is depicted in Fig. 2. For the small-diameter shield ($D_s/D_c = 1.3$, ○), the resonant frequency can be changed by over 40 MHz. The highest resonant frequency is achieved when the shield is symmetric about longitudinal axis of the coil ($z = 0$ mm). With the larger shield diameter ($D_s/D_c = 1.5$, ●) the tuning range decreases by a factor of 2 because of the increase in the effective mutual inductance. Decreasing the shield diameter effectively increases the tuning range at the expense of B_1 field magnitude (*8, 9*). The D_s/D_c ratio was 1.5 for the coil pictured in Fig. 3.

Figure 4a does not include the coupling effects of the microimaging gradient insert. When the gradient insert is included the tunable range is reduced from 20 to 7 MHz for

FIG. 3. (a) Photograph depicting low-pass birdcage RF coil built using disc capacitors and (b) RF coil with an adjustable RF shield used for tuning.

FIG. 4. (a) Graph of frequency change vs shield position (z) *without* the microimaging gradients in place. The frequency change vs shield position curve for the small-diameter shield, D_s, when compared to the diameter of the RF coil, D_c ($D_s/D_c = 1.3$, ○), and frequency change vs shield position curve for when the shield diameter is 1.5 times the coil diameter ($D_s/D_c = 1.5$, ●). Increasing the shield diameter increases the effective inductance and reduces the tuning range by one-half. (b) Plot of resonant frequency vs shield position (z) for the RF probe *with* the microimaging gradients and $D_s/D_c = 1.5$. Measurements were made using the same experimental configuration as for *in vivo* microimaging. Plot of resonant frequency vs shield position (z) of the unloaded coil (●) and when the RF coil was fully loaded with 9 ml of a 5 mM copper sulfate solution (○). The measured Q was 600 and 500 for the unloaded and loaded coil, respectively. The dashed line represents the desired resonant frequency.

the large-diameter shield ($D_s/D_c = 1.5$) (Fig. 4b). The two curves depict resonant frequency when the coil was both loaded and unloaded. The Q for the unloaded coil was 635 and was lowered to 490 for the fully loaded coil (9 ml of 5 mM CuSO$_4$ solution). For the standard manufacturer's high-resolution 25-mm-diameter probe, the unloaded and loaded Q were 440 and 370, respectively. This represents a 15% increase in the SNR for the RF shield tunable probe when compared to the standard microimaging probe. The Q value was similar when the coil was loaded with the head of a 12-g, 7-day-old neonatal rat pup. Although the frequency range can be increased with a smaller diameter RF shield, the center field magnitude is reduced by 25% when compared to a shield with a larger diameter (8).
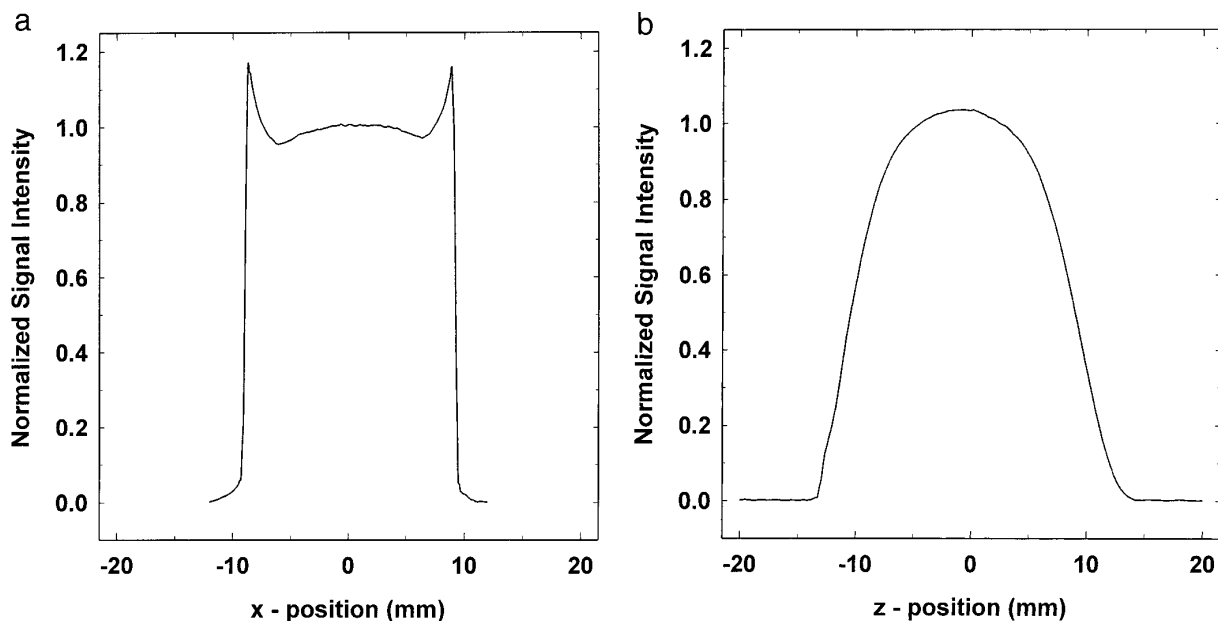
Experimental results from images are illustrated in Figs. 5 and 6. Figure 5a is a plot of the magnitude signal intensity taken from an axial (x direction) spin-echo profile (20-mm-diameter phantom; 9 ml of 5 mM CuSO$_4$-doped H$_2$O). The intensity is very uniform over 18 mm of the coil diameter. The peaks at the edges of the profile were due to the increased leg currents in the elements through which this profile was obtained. Figure 5b shows signal intensity taken from a longitudinal profile of the same phantom along the z axis which was parallel to B_0. Again the signal intensity is quite uniform over 20 mm in length.

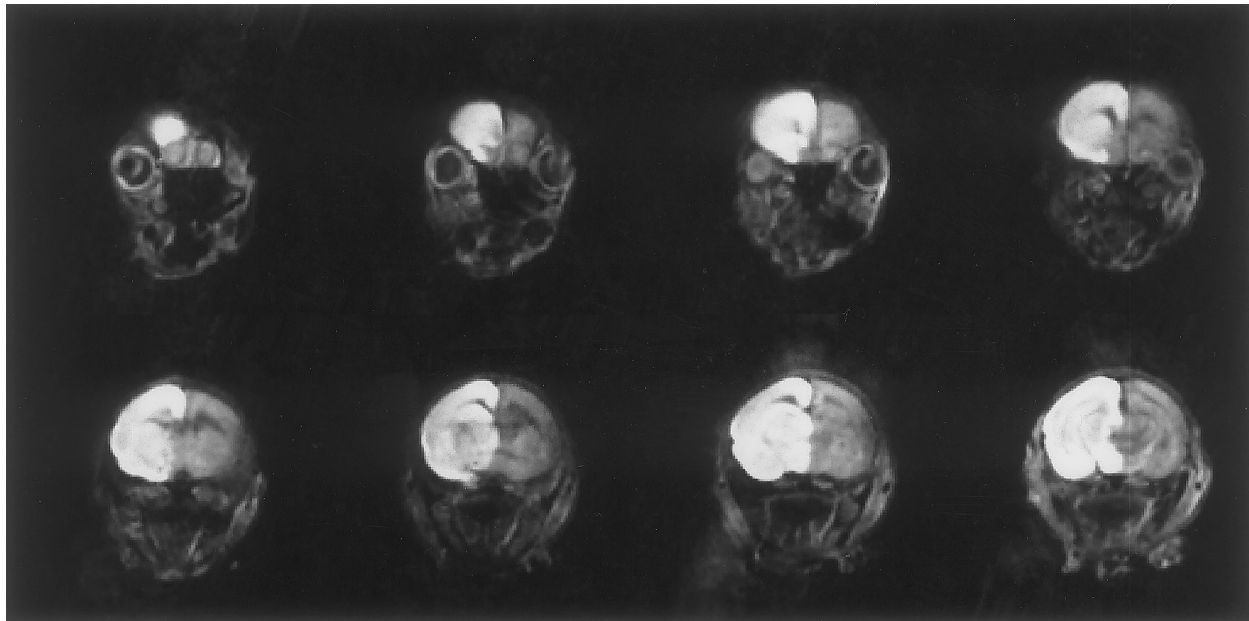The goal for the design and construction of this probe was

in vivo microimaging. An example of a contiguous multislice diffusion-weighted image of a 7-day-old rat pup brain is shown in Fig. 6. These images have a typical SNR of greater than 400 and illustrate the utility of this design. Animals can be exchanged by removal of the probe insert (RF probe only) from the bottom of the magnet in less than 5 min. Images depict excellent B_1 field homogeneity with no signal loss or distortion associated with other designs employing adjustable tuning capacitors.

To simulate the effects of the adjustable RF shield used for tuning on B_1 homogeneity, 3D field calculations were performed on a model of the coil derived from the experimental coil. Figure 7 demonstrates contour plots of the B_1 field intensity through the longitudinal axis of the RF coil for the case when the RF coil is shielded by the adjustable RF shield in three different configurations. Shown are B_1 field distributions for the large-diameter ($D_s/D_c = 1.5$) asymmetric ($z = 13$ mm) RF shield in Fig. 7a, the large symmetric shield ($z = 0.0$ mm) in Fig. 7b, and the small ($D_s/D_c = 1.3$) asymmetric shield ($z = 13$ mm) in Fig 7c.
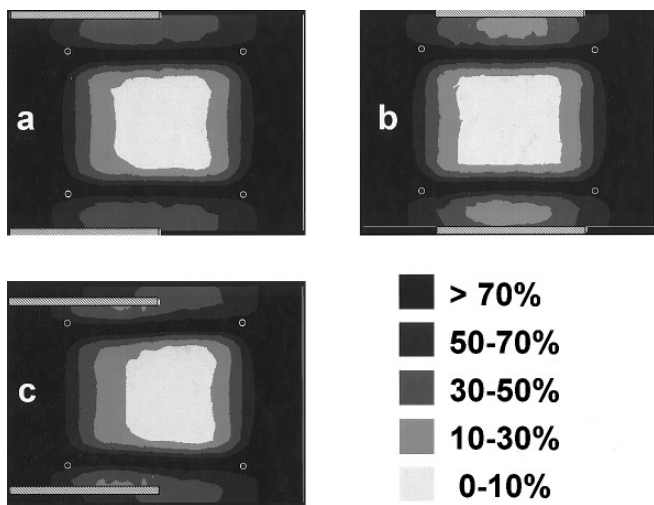
Calculations of the area and centroid of the 0–10% B_1 homogenous region from Fig. 7 are given in Table 1 and provide a more quantitative comparison between the three cases. For the large asymmetric shield, the 0–10% homogenous region increases by 3.8% and the centroid is skewed to the right from the true center by 3.5%. For the large

FIG. 5. (a) Profile of normalized signal intensity vs short axis (x) position of the RF coil. This profile was obtained from a spin-echo image acquired in the central axial ($x–y$) plane in order to demonstrate B_1 field homogeneity. The field of view was 24 mm. The peaks at the edges of the profile are due to the current in the leg elements through which this profile was obtained. (b) Profile of normalized signal intensity vs longitudinal (z) position of the RF coil. This profile was obtained from a spin-echo image acquired in the central sagittal ($x–z$) plane in order to demonstrate B_1 field homogeneity. The field of view was 40 mm.

FIG. 6. Diffusion-weighted magnetic resonance images of a 7-day-old neonatal rat pup subjected to 3 h of hypoxia–ischemia to demonstrate image quality. Images were acquired 1 h post hypoxia–ischemia with a pulsed field gradient multislice interleaved spin-echo imaging sequence with TR/TE = 2000/70 ms, field of view = 24 mm, pixel resolution = 128 × 128, slice thickness = 1.0 mm, slice separation = 1.0 mm, number of averages = 2, bandwidth = 25 kHz, and b value = 1000 s/mm^2. The hyperintensity, ipsilateral to the right common carotid artery ligation, reflects the reduction in the apparent diffusion coefficient of endogenous tissue water accompanying cytotoxic edema. For more details on this animal model of neonatal hypoxia–ischemia consult Ref. (*12*).

FIG. 7. Simulated B_1 field contour plots derived from computer simulations. (a) B_1 field contour plots for $D_s/D_c = 1.5$ and $z = 13$ mm. (b) B_1 field contour plots for $D_s/D_c = 1.5$ and $z = 0$ mm. (c) B_1 field contour plots for $D_s/D_c = 1.3$ and $z = 13$ mm. The two cross-hatched white bars represent the RF shield position while the white circles indicate the end rings of the RF coil. The contours represent the relative deviations of the B_1 field when referenced to the field calculated at the center of the RF coil without an adjustable RF shield present. Included in these calculations but not shown is the long symmetric RF shield of the microimaging gradient insert.

symmetric shield, the 0–10% homogenous region increases by 13.3% with no skewing. For the small asymmetric shield, the 0–10% homogenous region is similar to an unshielded resonator, and the centroid of the homogenous region has a larger relative shift than that for the RF coil covered by the large asymmetric shield. Figure 7c and Table 1 indicate that a smaller asymmetric diameter shield will not improve homogeneity and will introduce a gradient in the RF profile or skewing of the contours toward the right of the geometrical center of the RF coil, away from the adjustable shield.

The results of the computer simulations in Table 1 and depicted in Fig. 7 are in reference to the 0–10% homogenous region of the same RF coil without any adjustable RF shielding but includes the shielding effect of the microimaging gradients.

Ignoring the shielding effects of the microimaging gradient insert decreases the overall B_1 field homogeneity and increases the skewing of the center contours (results not shown). Figure 7 indicates that the larger diameter adjustable shield will produce negligible experimental artifacts. Minimal differences between these two results can be attributed to the homogenizing effect of the long symmetric shield of the microimaging gradient insert.

The large adjustable RF shield can potentially reduce the center field strength by 13% (8) and therefore SNR when compared to the RF coil shielded by only the gradient insert. These calculations are based on the RF shield completely

covering the RF coil. For the work described here the SNR would be reduced by less than 13% since the adjustable shield partially covers the RF coil. Most coils used in microimaging are subject to similar shielding because of physical constraints. The RF homogeneity and convenience of tuning is worth this small loss in SNR.

The SNR can be improved by lowering the inductance of the conducting elements of the birdcage coil. This would also reduce the stray capacitance since larger leg capacitance would be needed for proper resonance. For the coil presented here, if the conducting element diameter is increased by 400% (decreasing the self-inductance by 68%), the leg capacitance necessary for proper resonance would only increase by 146% (3.3 to 4.8 pF). Optimization of the conducting element inductance and/or coil configuration would be necessary for operation above 400 MHz.

Another example of employing RF shield tuning was described by Lu and Joseph where they illustrate a technique for double-resonant operation in birdcage coils (4). Tuning was accomplished by inserting an additional RF shield of smaller diameter to increase the resonant frequency from ¹⁹F to ¹H. This configuration did not allow for continuously adjustable RF shield tuning, and this design still required adjustable tuning capacitors and physical electrical attachment. Birdcage coil tuning can be achieved by an adjustable diameter RF shield but would provide stringent physical limitations on coil construction.

SUMMARY

A simple effective low-pass birdcage coil which tunes through the application of a mechanically adjustable concentric RF shield was easily and inexpensively constructed for *in vivo* microimaging and spectroscopy. Tuning of the circuit was achieved by simply changing the overall effective induc-

TABLE 1
B_1 Field Homogeneity Calculations for an Adjustable RF Shield within the Microimaging Gradient

Tunable shield configuration and relative shield position[a]	B_1 field calculations (0–10%)[b] Homogenous region	
	Area change (%)	Centroid change (%)
$D_s/D_c = 1.5$, $z = 13$ mm	3.8	3.5
$D_s/D_c = 1.5$, $z = 0$ mm	13.3	−0.7
$D_s/D_c = 1.3$, $z = 13$ mm	0.5	9.7

Note. These data were derived from the contour plots shown in Fig. 7.

[a] The relative shield position (z) is defined as zero when the RF shield is symmetrically centered about the longitudinal axis of the RF coil, as measured from the geometrical center of the RF coil. D_s, adjustable shield diameter; D_c = RF coil diameter.

[b] All values are standardized to the resonator shielded by only the microimaging gradients.

tance by moving an RF shield about the longitudinal axis of an RF coil. The coil elements were made of only disc capacitors. Since the effective inductance for all the legs were equal, sources of B_1 field distortion and leg current imbalances caused by adjustable tuning and matching capacitors were eliminated. Matching was accomplished through inductive coupling. An RF shield diameter that is 1.5 times the diameter of the RF coil provides a solution with optimal B_1 field magnitude and homogeneity. This design produces an inexpensive isolated, physically unattached, resonant structure with an extremely homogenous B_1 field with a large Q and a tuning range of 7 MHz at 9.4 T. Similar designs would be applicable for systems with horizontal-bore magnets and systems operating at different static magnetic field strengths.

ACKNOWLEDGMENT

REFERENCES

1. C. E. Hayes, W. A. Edelstein, J. F. Schenck, O. M. Mueller, and M. Eash, An efficient, highly homogenous radiofrequency coil for whole-body NMR imaging at 1.5 T, *J. Magn. Reson.* **63,** 622–628 (1985).

2. J. Jin, G. Shen and T. Perkins, On the field homogeneity of a birdcage coil, *Magn. Reson. Med.* **32,** 418–422 (1994).

3. P. M. Joseph and D. Lu, A technique of double resonant operation of birdcage imaging coils, *IEEE Trans. Med. Imaging* **8,** 286–294 (1989).

4. D. Lu and P. M. Joseph, A technique of double-resonant operation of ^{19}F and ^{1}H quadrature birdcage coils, *Magn. Reson. Med.* **19,** 180–185 (1991).

5. R. Pascone, T. Vullo, J. Farelly, and P. T. Cahill, Explicit treatment of mutual inductance in eight-column birdcage resonators, *Magn. Reson. Imaging* **10,** 401–410 (1992).

6. J. Jin, G. Shen, and T. Perkins, A simple method to incorporate the effects of an RF shield into RF resonator analysis for MRI applications, *IEEE Trans. Biomed. Eng.* **42,** 840–843 (1995).

7. M. C. Leifer, Resonant modes of the birdcage coil, *J. Magn. Reson.* **124,** 51–60 (1997).

8. C. M. Collins, S. Li, Q. X. Yang, and M. B. Smith, A method for accurate calculation of B_1 fields in three dimensions: Effects of shield geometry on field strength and homogeneity in the birdcage coil, *J. Magn. Reson.* **125,** 233–241 (1997).

9. S. Crozier, L. K. Forbes, W. U. Roffmann, K. Luescher, and D. M. Doddrell, Currents and fields in shielded RF resonators for NMR/MRI, *Meas. Sci. Technol.* **7,** 1083–1086 (1996).

10. J. Tropp, The theory of the birdcage resonator, *J. Magn. Reson.* **82,** 51–62 (1989).

11. J. Tropp and F. S. Huang, Prediction of frequency shifts for the shielded bird cage, *in* Abstracts of the Society of Magnetic Resonance in Medicine, 12th Annual Meeting, New York, p. 1348 (1993).

12. J. E. Rice, R. C. Vannucci, and J. B. Brierly, The influence of immaturity on hypoxic–ischemic brain damage in the rat, *Ann. Neurol.* **9,** 131–141 (1981).